World Academy of Science, Engineering and Technology
International Journal of Aerospace and Mechanical Engineering
Vol:7, No:6, 2013

Numerical Evaluation of the Contribution of Inertial and Aerodynamic Forces on VAWT Blade Loading

Marco Raciti Castelli, Stefano De Betta, and Ernesto Benini

Abstract—A two-dimensional numerical simulation of the contribution of both inertial and aerodynamic forces on the blade loads of a Vertical-Axis Wind Turbine (VAWT) is presented. After describing the computational model and the relative validation procedure, a complete campaign of simulations - based on full RANS unsteady calculations - is proposed for a three-bladed rotor architecture characterized by a NACA 0021 airfoil. For each analyzed angular velocity, the combined effect of pressure and viscous forces acting on every rotor blade are compared to the corresponding centrifugal forces, due to the revolution of the turbine, thus achieving a preliminary estimation of the correlation between overall rotor efficiency and structural blade loads.

Keywords—CFD, VAWT, NACA 0021, aerodynamic forces, inertial loadings.

I. Introduction and Background

EUROPE gets approximately 20% of its electricity from renewable energy sources, including 5.3% from wind energy. That share will increase up to 2020 when, under the terms of the EU renewable energy directive, which sets legally binding targets for renewable energy in Europe, 34% of the EU total electricity consumption will come from renewable energy sources, with wind energy accounting for 14% [1]. In this scenario, the research in wind energy systems acquires considerable importance. This continuous quest for clean energy is now focusing on the local production of electric power, spread in a wide area, so as to cooperate with the big electric power plants, centralized in just few specific strategic locations of the countries. One of the most promising resources is wind power associated with local production of clean electric power inside the built environment, such as industrial and residential areas, which has lead to the development of the so called computational wind engineering. The new discipline has also renewed the interest in vertical axis wind turbines (VAWTs) [2]. The use of building mounted wind turbines, specifically on mid to high-rise urban buildings, has displayed some distinct benefits for small scale wind energy generation. These benefits include: local energy production and consumption, reduced capital investment in towers and transmission lines, as well as increased wind speeds around buildings, thus producing a higher amount of energy [3].

A number of features have determined horizontal-axis wind turbines (HAWTs) to be preferred and become the dominant design type, especially in the utility-scale (large and very large turbines) segment. But, in certain conditions (sites with highly turbulent wind, like in the mountains or inside the urban environment), VAWTs seem to offer a better solution for the wind energy harnessing [4]. Many factors play a role in the design of a wind turbine rotor, including aerodynamics, generator characteristics, blade strength and rigidity, noise levels. But, since the success of a small wind energy conversion system is largely dependent on maximizing its energy extraction, rotor aerodynamics play a critical role in the minimization of the cost of energy [5]. A widely used way to improve the aerodynamics of wind turbines is the utilization of computational fluid dynamics (CFD), which is definetly less expensive than experimental tests.

Mc Laren et al. [6] pointed out that the dynamic loading on the blades of the turbines, as they rotate about the central shaft and travel trough a wide range of relative angles of attack, is expected to produce significant deflections of the turbine blades. This could result in appreciable noise generation, as well as an increase in the potential fatigue failure. In fact, the majority of the lift and drag forces acting on rotor blades are in the radial direction. Numerical simulations were performed with the steady state approximation of the flow near a VAWT, allowing the prediction of the general trends and relative force magnitudes, but proved to be unable to fully capture the complexity of the flow.

Mc Laren et al. [7] also performed a series of full scale experimental wind tunnel tests to determine the aerodynamic loading on the airfoil of a three-bladed VAWT characterized by high solidity and low rotational speed. A large peak in thrust and radial force was observed during the upstream portion of blade revolution, as the airfoil lift increases along with the relative angle of attack. It was also noticed that the vibration exciting radial load amplitude is typically on the order of five times greater than that of the power producing thrust load.

In this work the aerodynamic and inertial loads acting on a VAWT blade are investigated. A moving mesh is adopted to study the behavior of a three-bladed rotor, revolving at different values of the tip speed ratio. The resultant aerodynamic loads are compared with inertial forces generated by the rotation of the blades. Also a comparison of the intensity of normal and tangential forces is performed, in order to determine the values of angular position where energy extraction is higher.

II. Model Geometry

The aim of the present work is to numerically analyze the aerodynamic behavior of a three-bladed Darrieus VAWT operating at different angular velocities, for a constant wind speed

Marco Raciti Castelli is a Research Associate at the Department of Industrial Engineering of the University of Padua, Via Venezia 1, 35131 Padua, Italy (e-mail: marco.raciticastelli@unipd.it).

Stefano De Betta is an Aerodynamic Researcher at HIT09 S.r.l., Galleria Storione 8, 35131 Padua, Italy.

Ernesto Benini is an Associate Professor at the Department of Industrial Engineering of the University of Padua, Via Venezia 1, 35131 Padua, Italy (email: ernesto.benini@unipd.it).

of 9 m/s. The main features of the turbine are summarized in Table 1. Rotor azimuthal position is identified by the angular coordinate of the pressure centre of blade No. 1 (set at 0.25c for NACA 0021 airfoil), starting between the 2^{nd} and 3^{rd} Cartesian plane octants, as can be seen from Fig. 1.

TABLE I
MAIN GEOMETRICAL FEATURES OF THE TESTED MODEL

D_{rotor} [mm]	1030
H_{rotor} [mm]	1 (2D simulation)
Blade profile	NACA 0021
c [mm]	85.8

III. Description of the Numerical Flow Field

As the aim of the present work is to reproduce the operation of a rotating machine, the use of moving sub-grids is necessary. In particular, the discretization of the computational domain into macro-areas leads to two distinct sub-grids:

- a rectangular outer zone, determining the overall calculation domain, with a circular opening centered on the turbine rotational axis, which is identified as *Wind Tunnel sub-grid*, fixed;
- a circular inner zone, which is identified as *Rotor sub-grid*, rotating with rotor angular velocity ω.

Fig. 2 shows the main dimensions of the *Wind tunnel sub-grid* area.

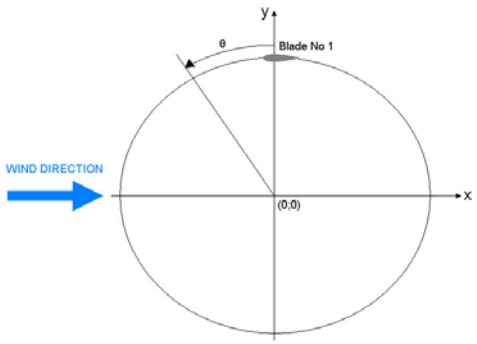

Fig. 1. Azimuthal coordinate of the centre of pressure of rotor blade No. 1

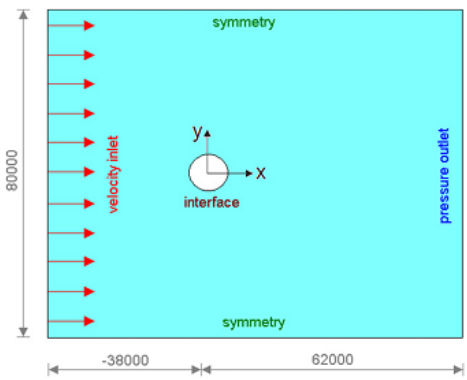

Fig. 2. Main dimensions [mm] of the *Wind Tunnel sub-grid* area

In order to allow a full development of the wake, Ferreira et al. [8] placed inlet and outlet boundary conditions respectively 10 diameters upwind and 14 diameters downwind with respect to rotor test section for a wind tunnel CFD simulation. As the aim of the present work is the simulation of a turbine operating in open field conditions and because of the huge domain width necessary to avoid solid blockage, inlet and outlet are placed respectively 37 rotor diameters upwind and 60 rotor diameters downwind with regard to the rotor test section. Inlet is set as a *velocity inlet*, with a constant velocity profile of 9 m/s, while outlet is set as a *pressure outlet*. Two symmetry boundary conditions are adopted for the two side walls. The circumference around the circular opening, centered on the turbine rotational axis, is set as an *interface*, thus ensuring the continuity in the flow field.

The *Rotor sub-grid* is the fluid area simulating the revolution of the wind turbine and is therefore characterized by a moving mesh, rotating at the same angular velocity of the turbine. Its location coincides exactly with the circular opening inside the *Wind Tunnel sub-grid* area and is centered on the turbine rotational axis. Fig. 3 shows the main dimensions and the boundary conditions of the *Rotor sub-grid* area.

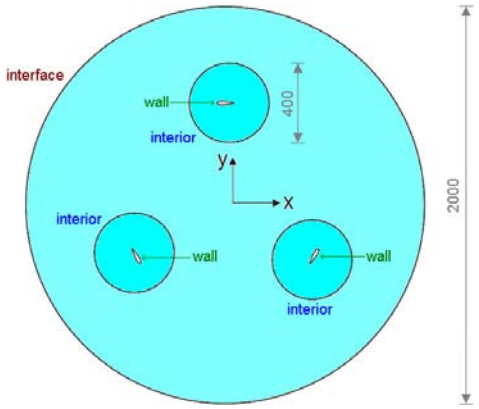

Fig. 3. Schema of the *Rotor sub-grid* area [mm]

All the blade profiles inside the *Rotor sub-grid* area are enclosed in a control circle of 400 mm diameter. Unlike the *interface*, it has no physical significance: its aim is to allow a precise dimensional control of the grid elements in the area close to rotor blades, by adopting a first size function operating from the blade profile to the control circle itself and a second size function operating from the control circle to the whole *Rotor sub-grid* area, ending with grid elements of the same size of the corresponding *Wind Tunnel sub grid* elements. An *interior* boundary condition is used for control circle borders, thus ensuring the continuity of the cells on both sides of the mesh.

IV. Discretization of the Numerical Flow Field

A rotating mesh is adopted in order to represent the revolving motion of the VAWT. To discretize the flow field, an unstructured grid is chosen for the entire domain, in order to reduce the engineering time to prepare the CFD simulations. The mesh on both sides of the *interface* (*Rotor*

sub-grid and *Wind Tunnel sub-grid* areas) has approximately the same characteristic cell size, in order to obtain faster convergence [9].

An isotropic unstructured mesh is chosen for the *Rotor sub-grid*, in order to guarantee the same accuracy in the prediction of rotors performance during the revolution of the turbine (according to the studies of Commings et al. [10]) and also in order to test the prediction capability of a very simple grid. Considering their features of flexibility and adaption capability, unstructured meshes are in fact very easy to obtain, for complex geometries, too, and often represent the first attempt in order to get a quick response from the CFD in engineering work.

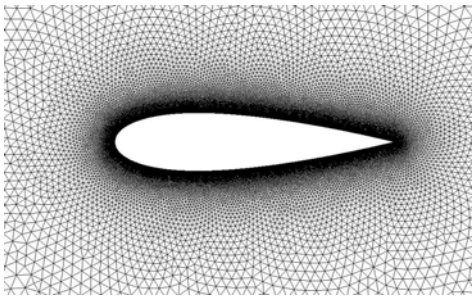

Fig. 4. Spatial domain discretization near the NACA 0021 blade section

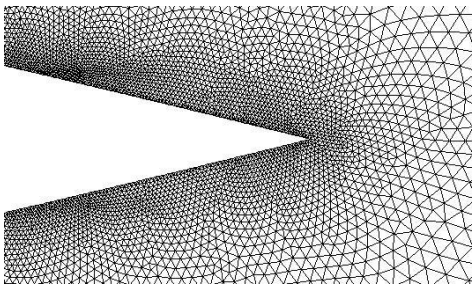

Fig. 5. Spatial domain discretization close to airfoil trailing edge

TABLE II
MAIN FEATURES OF THE MESH CLOSE TO ROTOR BLADE

Number of grid points on airfoil upper/lower surface [-]	3600
Minimum grid spacing (on airfoil leading edge) [mm]	0.015
Maximum grid spacing (on airfoil trailing edge) [mm]	0.025
Growth factor from leading edge to trailing edge [-]	1.005
Growth factor from airfoil surface to *Rotor sub-grid* [-]	1.1

Being the area close to the blade profiles, great attention is placed in the *control circle*. The computational grids are constructed from lower topologies to higher ones, adopting appropriate size functions, in order to cluster grid points near the leading edge and the trailing edge of the blade profile, so as to improve the CFD code capability of determining lift, drag and the separation of the flow from the blade itself. Table II summarizes the main features of the mesh close to rotor blade, Fig. 4 shows the mesh near the airfoil while Fig. 5 displays the mesh close to its trailing edge. In order to determine the optimal size of the near wall cells, a statistical analysis of the y^+ parameter was previously performed. For further information about mesh generation and code validation, see [11]. For the proposed computations, the dimension of the near-wall mesh determines mean values of y^+ between 1 and 5.

V. Main Features of the Numerical Simulation

A complete campaign of simulations, based on full RANS unsteady calculations, is performed for a threee-bladed rotor architecture characterized by a NACA 0021 airfoil. The tip speed ratio, defined as:

$$\lambda = \omega R_{rotor}/V_\infty \tag{1}$$

is varied from a value of $\lambda = 1.44$ (which corresponds to an angular velocity of $\omega = 25.1$ rad/s) to $\lambda = 3.3$ (which corresponds to an angular velocity of $\omega = 57.6$ rad/s). These conditions correspond to a range of blade Reynolds numbers from $7.77 \cdot 10^4$ to $1.78 \cdot 10^5$, being the blade Reynolds number defined as:

$$Re = \rho \omega R_{rotor}/\mu \tag{2}$$

The dynamic viscosity μ is assumed to be $1.78 \cdot 10^{-5}$ Pa·s, the density ρ is set to 1.225 kg/m^3 and the free stream velocity V_∞ is set to 9 m/s.

VI. Numerical Solution

As pointed out by Mc Muller et al. [12], the calculation of unsteady flows in turbomachinery continues to present a severe challenge to CFD. During VAWT operation, the unsteadyness stems mainly from the relative motion of the rotating blade and has a fundamental period which depends both on the rate of rotation and on the number of blades. For the proposed calculations, the temporal discretization is achieved by imposing a physical time step equal to the lapse of time the rotor takes to make a 1° rotation.

As a global convergence criterion, each simulation is run until instantaneous torque values show a deviation of less than 1% compared with the equivalent values of the previous period, for three consecutive periods. Residuals convergence criterion for each physical time step is set to 10^{-5} [11].

The adopted turbulence model is *enhanced k- realizable*. This choice is made after a series of analysis [11] that pointed out that the selected turbulence model well suits with the numerical simulation of a Darrieus VAWT. A 2D pressure based solver is adopted, which is well suited to solve incompressible flows [9]. The unsteady formulation is set to second-order implicit.

VII. Results and Discussion

As shown in Fig. 6, the aerodynamic force acting on each rotor blade can be decomposed in a component tangent to the chord, the tangential force F_t, and a component perpendicular to the chord, the radial force F_n. The radial force is considered positive when pointing outwards with respect to the rotational

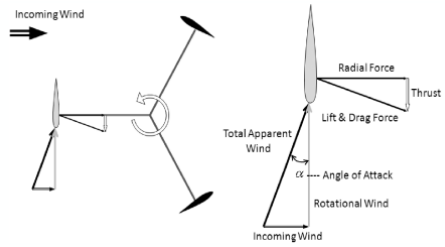

Fig. 6. Schematic representation of VAWT principle of operation (from: [3])

axis and does not produce any effect on the torque of the rotor, wehreas its amplitude causes structural loads.

The centrifugal force is defined as

$$F_c = mR_{rotor}\omega^2 \tag{3}$$

where m is the mass of the blade, set to 0.55 kg, R_{rotor} is the rotor radius and ω is its angular velocity. This force acts in the same direction of the radial force, always pointing outwards with respect to the rotational axis.

Figs. from 7 to 14 show a comparison between the aerodynamic radial force and the centrifugal one, acting on rotor blade No. 1 during a complete revolution, for all the analyzed tip speed ratio. In each figure, the values of radial force (F_n), centrifugal force (F_c) and their sum (F_{tot}) are represented.

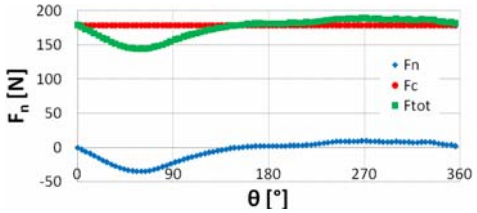

Fig. 7. Normal force F_n, centrifugal force F_c and total radial resultant force F_{tot} for $\lambda = 1.44$.

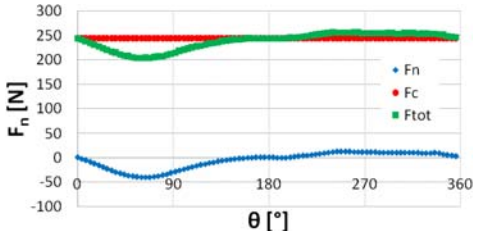

Fig. 8. Normal force F_n, centrifugal force F_c and total radial resultant force F_{tot} for $\lambda = 1.68$.

Fig. 15 represents the ratio between the normal (aerodynamic) and the centrifugal (inertial) forces acting on a single blade for all the tested values of the tip speed ratio. As can be clearly seen, the contribution of the inertial force on the global blade loading is predominant.

The tangential component of the aerodynamic force acting on each blade, F_t, is responsible for the motion of the rotor. In Fig. 16 the ratio F_t/F_n is plotted as a function of the azimuthal position for all the examined tip speed ratios. It can be seen that the ratio is lower than 1 for almost all the values of θ, except when the airfoil travels close to $\theta = 0°$ and $\theta = 180°$, being almost parallel to the incoming wind direction (in such conditions, the value of F_n tends to 0). This fact points out the intrinsically inefficient behavior of the

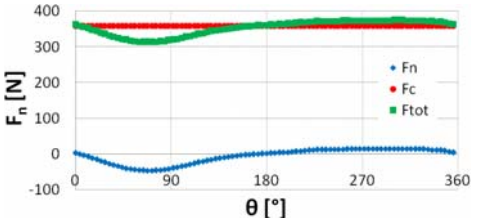

Fig. 9. Normal force F_n, centrifugal force F_c and total radial resultant force F_{tot} for $\lambda = 2.04$.

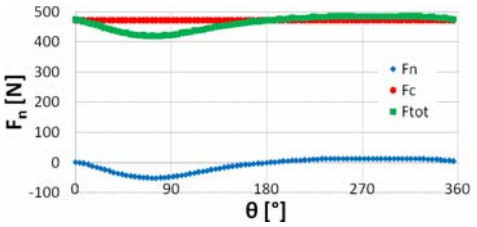

Fig. 10. Normal force F_n, centrifugal force F_c and total radial resultant force F_{tot} for $\lambda = 2.33$.

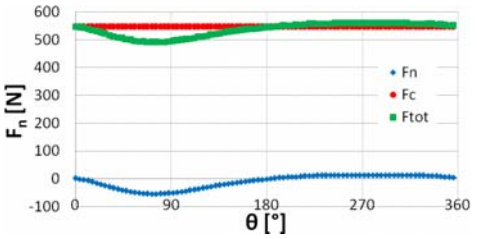

Fig. 11. Normal force F_n, centrifugal force F_c and total radial resultant force F_{tot} for $\lambda = 2.51$.

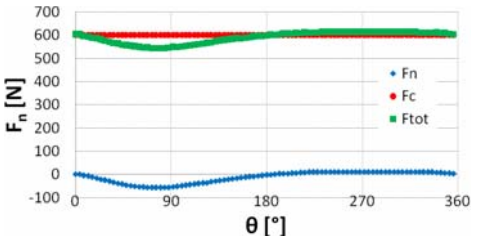

Fig. 12. Normal force F_n, centrifugal force F_c and total radial resultant force F_{tot} for $\lambda = 2.64$.

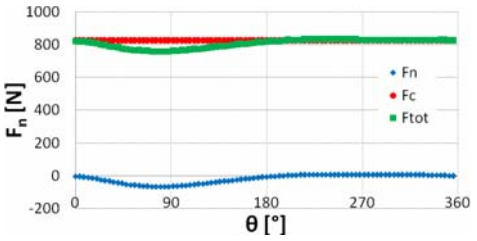

Fig. 13. Normal force F_n, centrifugal force F_c and total radial resultant force F_{tot} for $\lambda = 3.09$.

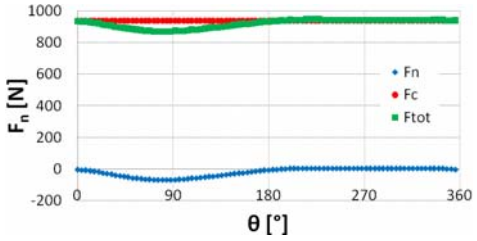

Fig. 14. Normal force F_n, centrifugal force F_c and total radial resultant force F_{tot} for $\lambda = 3.30$.

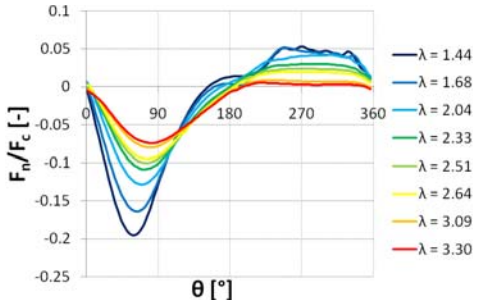

Fig. 15. Evolution of the ratio between normal and centrifugal force acting on a single blade, for different values of the tip speed ratio

Darrieus architecture. It can also be seen that, with the increase of the tip speed ratio, the turbine is less efficient in the upwind portion of blade revolution, but it results more efficient in the downwind phase. From this representation, it clearly appears that 90° angular position is quite efficient not only because of the amount of energy extracted from the fluid, but also thanks to the orientation of the force. In fact, a large component of the resultant aerodynamic force is oriented in the direction of the blade motion.

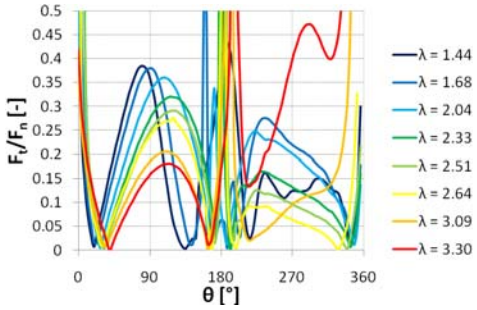

Fig. 16. Evolution of the ratio between tangential and normal force acting on a single blade for different values of the tip speed ratio

Fig. 17 presents the ratio between the average value of the tangential force during a full blade revolution and the absolute value of the average radial force, as a function of the ratio between the generic tip speed ratio and the tip speed ratio corresponding to the peak power coefficient. Once again, the intrinsically inefficient behavior of the Darrieus turbine can be noted. The peak of the graph is obtained for a tip speed ratio of about 85% of the optimal rotational speed, while the ratio corresponding to the tip speed ratio of peak power extraction is only 0.4. For higher values of λ, the ratio goes almost to zero.

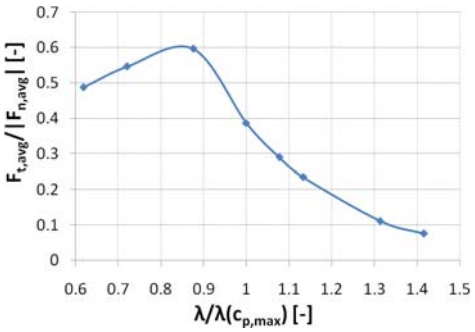

Fig. 17. Ratio between the average tangential force during a full blade revolution and the absolute value of the average radial force, as a function of $\lambda/\lambda_{(C_{p,max})}$

VIII. Conclusions

A series of numerical analyses on a three-bladed VAWT have been performed in order to compare the effects of inertial and aerodynamic forces acting on the rotor blade. The aerodynamic radial force has been compared with the centrifugal one, the latter resulting large enough to overcome the compression peaks due to the aerodynamic force. As a result, the blade is always pushed outwards. Also the ratio between radial and inertial forces has been studied, proving that its peak becomes smaller with the increase of the rotational speed, being also shifted to higher values of the azimuthal position. Finally, the intrinsically inefficient behavior of the Darrieus VAWT has been highlighted through the ratio between the tangential force and the radial one: the radial component of the resultant aerodynamic force always exceeds the tangential one, which is responsible for the motion of the turbine.

Nomenclature

A [m^2]	rotor swept area
c [m]	chord length
D_{rotor} [m]	rotor diameter
F_c [N]	centrifugal force
F_n [N]	aerodynamic radial force
F_t [N]	aerodynamic tangential force
H_{rotor} [m]	rotor height
m [kg]	blade mass
Re [-]	Reynolds number
R_{rotor} [m]	rotor radius
V_∞ [m/s]	freestream wind velocity
θ [°]	azimuthal position
λ [-]	tip speed ratio
μ [Pa·s]	dynamic viscosity
ρ [kg/m^3]	air density
ω [rad/s]	rotor angular velocity

References

[1] European Wind Energy Association, EU energy policy after 2020, *www.ewea.org*, 2011.
[2] M. Raciti Castelli, E. Benini, "Effect of blade inclination angle on a Darrieus wind turbine", *Journal of turbomachinery*, Vol. 134, May 2012, 031016-1-10.

[3] S. J. Kooiman, S. W. Tullis, "Responce of a Vertical Axis Wind Turbine to Time Varying Wind Conditions found within the Urban Environment", *Wind Engineering*, Vol. 34, No. 4, 2010.
[4] I. Paraschivoiu, O. Trifu, F. Saeed, "H-Darrieus Wind Turbine with Blade Pitch Control", *International Journal or Rotating Machinery*, Vol. 2009 (2009), ID 505343.
[5] M. Dunquette, K. Visser, "Numerical Implications of Solidity and Blade Number on Rotor Performance of Horizontal-Axis Wind Turbines", *Journal of Solar Energy Engineering*, 125(4), pp. 425-432, November 2003.
[6] K. McLaren, S. Tullis, S. Ziada, "CFD Simulation of Dynamic Thrust and Radial Forces on a Vertical Axis Wind Turbine Blade", *The 15th Annual Conference of the CFD Society of Canada*, Toronto, Canada, 2007.
[7] K. McLaren, S. Tullis, S. Ziada, "Vibrational response behavior of a high solidity, low rotational velocity, vertical axis wind turbine", *Proceeding of ASME 2010 3rd joint US-European Fluids Engineering Summer Meeting and 8th International Conference on Nanochannel, Microchannels and Minichannels*, Montreal, Canada, August 2-4, 2010.
[8] S. Ferreira, H. Gijl, G. van Bussel, G. van Kuik, "Simulating dynamic stall in a 2D VAWT: modeling strategy, verification and validation with particle image velocimetry data", *The Science of making torque from wind. Journal of Physics: Conference Series* 75, 2007.
[9] Fluent Inc., *Fluent Users Manual*,pp. 193-194, 2006.
[10] R. M. Cummings, J. R. Forsythe, S. A. Morton, K. D. Squires, "Computational challenges in high angle of attack flow prediction", *Prog Aerospace Sci*, 2003.
[11] M. Raciti Castelli, G. Ardizzon, L. Battisti, E. Benini, G. Pavesi, "Modeling strategy and numerical validation for a darrieus vertical axis micro-wind turbine", *Proceeding of ASME 2010 International Mechanichal Engineering ongress & Exposition IMECE2010*, Vancouver, Canada, November 12-18, 2010.
[12] M. McMullen, A. Jameson, J. J. Alonso, "Acceleration of convergence to a periodic steady state in turbomachinery flows", *Proceeding of the 39th AIAA Aerospace Sciences Meeting & Exhibit*, January 8-11, 2001, Reno, NV.